THE JOURNAL OF PHYSICAL CHEMISTRY B

ARTICLE

pubs.acs.org/JPCB

# Novel Polypropylene/Inorganic Fullerene-like $WS_2$ Nanocomposites Containing a $\beta$-Nucleating Agent: Dynamic Crystallization and Melting Behavior

Mohammed Naffakh,* Carlos Marco, and Gary Ellis

Instituto de Ciencia y Tecnología de Polímeros, ICTP-CSIC, c/Juan de la Cierva, 3, 28006, Madrid, Spain

**ABSTRACT:** The dynamic crystallization and melting behavior of isotactic polypropylene−tungsten disulfide (iPP/IF-$WS_2$) nanocomposites incorporating a $\beta$-nucleating agent is investigated by X-ray diffraction and differential scanning calorimetry. A conventional melt-processing strategy is employed to generate new materials that exhibit variable $\alpha$ and $\beta$ polymorphism under the appropriate kinetic conditions. The results show that when the dual additive system is employed the nucleation ability on isotactic polypropylene not only depends on the nucleation efficiency (NE) and relative content of the individual $\alpha$ and $\beta$-nucleating agents, but also on the cooling rates employed. The nucleating behavior of the additives is explained by competitive nucleation, and the correlation between crystallization and melting temperatures and relative content of $\alpha$ and $\beta$-crystals of iPP in the nanocomposites is discussed.

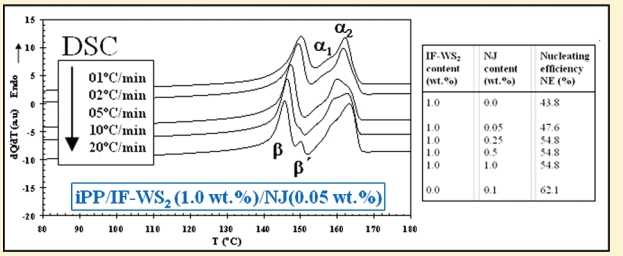


## 1. INTRODUCTION

Polypropylene is one of the most highly consumed plastic materials in the world, and its high versatility and cost competitiveness has led to continued sustainable growth over the past decade. Crystallization is one of the most important variables in the production of polypropylene-based materials, and for many years this process has been modified and promoted through the use of specific heterogeneous nucleating additives.[1−9] Such nucleating agents (NAs) not only lead to an increase in the rate of production of polymer articles but they can also significantly alter the solid-state structure and consequently broaden the spectrum of the materials characteristics such stiffness, ductility, clarity, and transparency.[7−9] Specific nucleators for isotactic polypropylene (iPP) are available that can induce predominant formation of the most widespread $\alpha$-phase, the trigonal $\beta$-phase, or the less-common $\gamma$-phase.[4,6,9] The $\alpha$-phase is the thermodynamically stable crystalline form and hence the most common modification of iPP. However, the lower melting temperature and density of $\beta$-iPP make this modification an interesting alternative to the $\alpha$-iPP for specific applications. With respect to application properties, $\alpha$-nucleating agents can improve tensile and flexural behavior as well as the transparency of iPP, while $\beta$-nucleating agents can improve the impact strength and heat distortion temperature of iPP, albeit at the expense of stiffness.[10−14] In this respect, combining $\alpha$- and $\beta$-nucleating agents as a strategy to obtain controlled adjustment of stiffness and toughness of iPP is very interesting from both scientific and industrial viewpoints.[15−19] However, controlled tailoring of iPP properties requires some insight into the relationships between the different nucleating agents, crystallization properties, crystal structure, and mechanical properties. In this respect, the identification of which nucleating agent dominates the crystallization process, and the understanding of the factors affecting the nucleation behavior when dual $\alpha/\beta$ nucleating agents are employed, are of fundamental interest.

However, in order to expand the engineering uses of iPP extensive efforts have been made to improve its thermal and mechanical properties through compounding with nanoscaled reinforcements, mainly because the large specific surface area of nanoparticles leads to strong interfacial interactions with the surrounding polymer matrix, and is effective for the improvement of the mechanical properties of polymers. Among the many nanoreinforcements employed in polypropylene, such as montmorillonite clays, $CaCO_3$, silica, carbon nanotubes, inorganic fullerenes, carbon nitrides, inorganic nanotubes, etc.,[20−28] inorganic fullerene tungsten disulfide (IF-$WS_2$) nanoparticles have been shown to be efficient for improving the thermal, mechanical, and tribological properties in a number of thermoplastic polymers, including isotactic polypropylene (iPP),[24,25] polyphenylene sulfide (PPS),[29] poly(ether ether ketone) (PEEK),[30] nylon-6,[31] that were processed via traditional melt processing techniques as economical and scalable routes, without the need for modifiers, surfactants, or dispersing agents. In particular, the incorporation of IF-$WS_2$ into the iPP has shown to be very efficient in improving the thermal stability, storage modulus, and crystallization behavior of the polymer matrix due to the highly efficient nucleating ability of IF-$WS_2$ on the monoclinic $\alpha$-form crystals.[24]

More recently, a number of innovative approaches based on the use of both micro- and nano-particles,[32,33] as well dual-nanoparticles with different characteristics,[34,35] have been described that exploit synergistic effects to produce new materials

**Received:** June 21, 2011
**Revised:** August 2, 2011
**Published:** August 08, 2011

with enhanced properties. In the present work, the preparation of new iPP nanocomposites incorporating IF-$WS_2$ nanoparticles and a commercially available $\beta$-nucleating agent is described, the effect of the $\alpha$(nano)/$\beta$(micro) concentration on the dynamic crystallization and melting of iPP is studied, and the nucleation efficiencies correlated with the polymorphic behavior of polypropylene in the nancomposite.

## 2. EXPERIMENTAL SECTION

**2.1. Materials and Processing.** Isotactic polypropylene (iPP) was provided by Repsol-YPF (Móstoles, Spain), with 95% isotacticity, a viscosity average molecular weight of 179 000 g/mol.[4] and a polydispersity of 4.77. The IF-$WS_2$ nanoparticles (NanoLub) were kindly supplied by Nanomaterials (Israel, known as ApNano Materials in the U.S.). The IF-$WS_2$ nanoparticles are multifaced polyhedra with an apparent shape ranging from spheres to ellipsoids. The particle aspect ratio ranges between 1 (spheres) and 2.3, with a mean value of 1.4, standard deviation of 0.3, and a median of 1.36. The particle dimensions are in the range of 40 to 200 nm with a mean value of 80 nm, standard deviation of 30 nm and median of 75 nm.[24] The $\beta$-nucleating agent was *N*,*N*′-dicyclohexyl-2,6-napthalene dicarboxamide (NJSTAR NU100), denominated NJ, kindly provided by RIKA International LTD (Manchester, U.K.).

Several concentrations of IF-$WS_2$ ($\alpha$) and NJ ($\beta$) ($\alpha/\beta$ = 1.0/0.05, 1.0/0.25, 1.0/0.50, and 1.0/1.0 wt.%) were introduced into the iPP matrix by melt-mixing using a microextruder (Thermo-Haake Minilab system) operated at 210 °C with a rotor speed of 150 rpm for 15 min. With the aim of improving the dispersion of the nanoparticles and $\beta$-nucleating agent in the matrix, IF-$WS_2$ was first introduced into the iPP matrix and mixed for 10 min, according to previous work.[24] Subsequently, the NJ nucleating agent was introduced into the extruder and mixing continued for anther 5 min. In addition, samples of neat iPP and binary systems of iPP/IF-$WS_2$ (1.0 wt.%) and iPP/NJ (0.1 wt %) were prepared under the same conditions.

**2.2. Characterization Techniques.** *2.2.1. Differential Scanning Calorimetry (DSC).* The crystallization and melting experiments were carried out using a Perkin-Elmer DSC7−7700 differential scanning calorimeter (Perkin-Elmer España SL, Madrid, Spain), calibrated with indium ($T_m$ = 156.6 °C, $\Delta H_m$ = 28.45 kJ/kg) and zinc ($T_m$ = 419.47 °C, $\Delta H_m$ = 108.37 kJ/kg). Aluminum capsules were employed with sample weights of approximately 10 mg studied under an inert nitrogen atmosphere with a flow rate of 25 mL/min. The thermal history prior to the crystallization of iPP was controlled by maintaining the samples in the melt for 5 min at a residence temperature of 210 °C, eliminating memory effects and assuring the maximum thermal stability of the components.[5]

Under dynamic conditions, cooling cycles from the melt were undertaken for each sample at cooling rates ($\phi$) of 1, 2, 5, 10, and 20 °C/min, followed by a heating cycle from 40 to 210 at 5 °C/min. The melting temperature ($T_m$) and the crystallization temperature ($T_p$) were determined at the maximum of the melting endotherm observed during the heating scan and the minimum of the crystallization exotherm observed during the cooling scan, respectively. Subsequently, the specific enthalpy of the $\alpha$-crystal form ($T_{m,\alpha}$) and $\beta$-crystal form ($T_{m,\beta}$) were calculated by the separation of the areas of the $\alpha$ and $\beta$ melting peaks according to the method recommended by Li and Cheung[36]

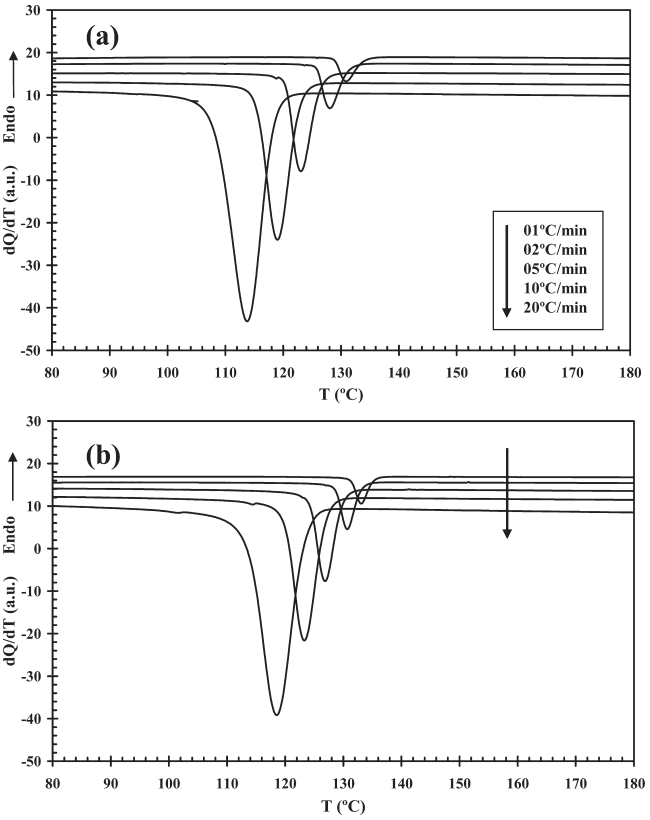


**Figure 1.** DSC thermograms of dynamic crystallization of (a) iPP/IF-$WS_2$ (1.0 wt.%) and (b) iPP/IF-$WS_2$ (1.0wt.%)/NJ(1.0 wt.%) obtained at the cooling rates indicated.

employing PeakFit software (Systat Software GmbH, Erkrath, Germany) for deconvolution. The crystallinity of the $\alpha$-form, $(1-\lambda)_\alpha$, and $\beta$-form $(1-\lambda)_\beta$, and the $\beta$-form content ($k_{DSC}$) were calculated as follows:

$$(1-\lambda)_\alpha = \frac{\Delta H_\alpha}{\Delta H^0_{m,\alpha}} \quad (1)$$

$$(1-\lambda)_\beta = \frac{\Delta H_\beta}{\Delta H^0_{m,\beta}} \quad (2)$$

$$k_{\beta,DSC} = \frac{\Delta H_\beta}{\Delta H_\alpha + \Delta H_\beta} \quad (3)$$

where $\Delta H^0_{m,\alpha}$ is the enthalpy fusion of 100% crystalline $\alpha$-iPP: 177 J/g, and $\Delta H^0_{m,\beta}$ is the enthalpy of 100% crystalline $\beta$-iPP: 168.5 J/g.[37]

*2.2.2. Wide Angle X-ray Diffraction (WAXS).* Wide-angle X-ray diffraction measurements (WAXS) were undertaken with a Bruker D8 Advance diffractometer (Bruker AXS GmbH, Karlsruhe, Germany) using Ni-filtered Cu$K_\alpha$ radiation, at a scan speed of 0.2°/s with a resolution of 40 points per degree over the angular region 2$\theta$ between 5 and 35°. Compression molded film samples were crystallized from the melt at 210 °C, at cooling rates of 2, 5, 10, and 20 °C/min in a Mettler FP90/FP82 HT temperature cell (Mettler-Toledo SAE, Barcelona, Spain).

The relative content of the $\beta$-form was estimated according to the procedure proposed by Turner-Jones et al.,[38] using the

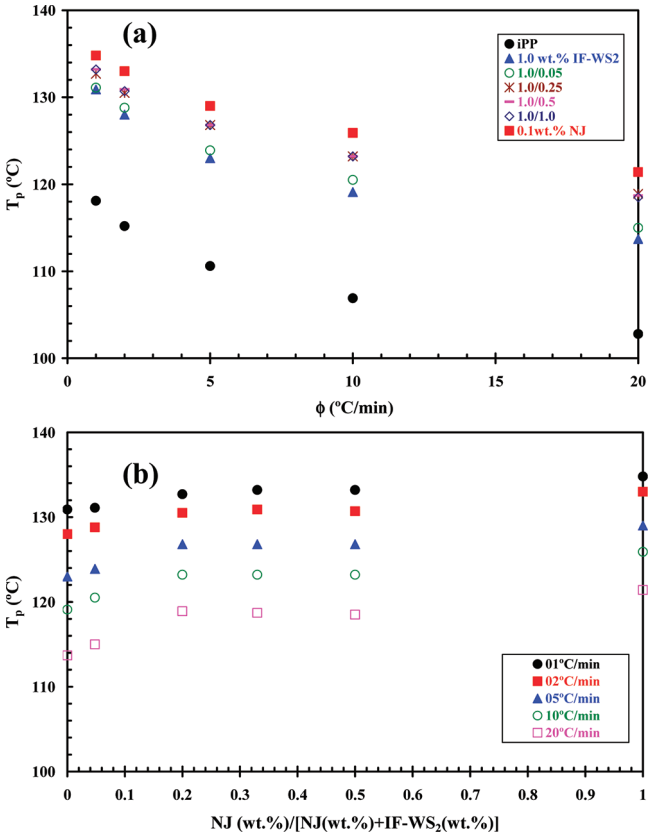


**Figure 2.** Variation of the crystallization peak temperature ($T_p$) with (a) the cooling rate and (b) the relative NJ content for iPP nucleated with dual $\alpha$(IF-$WS_2$)/$\beta$(NJ) NA and individual $\alpha$ or $\beta$ NA.

formula:

$$k_{\beta,\mathrm{WAXS}} = \frac{h_{\beta 1}}{h_{\beta 1} + h_{\alpha 1} + h_{\alpha 2} + h_{\alpha 3}} \quad (4)$$

Where $h_{\alpha 1}$, $h_{\alpha 2}$, $h_{\alpha 2}$ are the heights (from the top of the peak to the background curve) of three strong $\alpha$-form peaks (110), (040), and (130) at $2\theta = 14.1°$, 16.9°, and 18.8°, respectively, and $h_{\beta 1}$ is the height of the $\beta$- form peak (300) at $2\theta = 16°$.

## 3. RESULTS AND DISCUSSION

**3.1. Influence of the Cooling Rate and $\alpha$(IF-$WS_2$)/$\beta$(NJ) Concentration on the Crystallization Behavior of iPP.** The investigation of the nonisothermal crystallization behavior of iPP nucleated by individual and dual $\alpha$(IF-$WS_2$)/$\beta$(NJ) additives was undertaken by cooling the samples from the melt at different cooling rates, and the cooling curves recorded by DSC. As an example, Figure 1 shows the typical dynamic crystallization thermograms obtained at various cooling rates for iPP/IF-$WS_2$ (1.0 wt.%) and an iPP/IF-$WS_2$/NJ nanocomposite containing equal concentrations of IF-$WS_2$ and NJ (i.e., 1.0/1.0 wt.%). In both cases, the crystallization exotherms were observed to shift to lower temperatures and broaden as the cooling rate was increased. This is directly related to the formation of smaller crystals with a wider distribution of crystallite sizes. In particular, the corresponding crystallization temperature peak ($T_p$) at different cooling rates and relative NJ content were determined from the cooling curves, and the results are shown in Figure 2. Clearly, the data obtained show two salient features. First, the individual action of each additive, IF-$WS_2$ and NJ, on the nucleation of iPP and, second, the significant effect exerted by the NJ on the heterogeneous nucleation of iPP. Comparing the $T_p$ values of neat iPP and iPP nucleated by IF-$WS_2$ and NJ observed at a cooling rate of 10 °C/min, it can be seen that the nucleation effect of 0.1 wt.% of NJ is more important than that of 1.0 wt.% IF-$WS_2$ since $T_{p,\mathrm{iPP}}$ = 106.9 °C, $T_{p,1.0\mathrm{wt.\%\ IF\text{-}WS2}}$ = 119.9 °C and $T_{p,0.1\mathrm{wt.\%\ NJ}}$ = 125.9 °C. For iPP nucleated by IF-$WS_2$/NJ, the value of $T_p$ for iPP increases and tends to stabilize at concentrations greater or equal to 0.25%, where increments of around 16 °C in the value of $T_p$ were registered, Table 1. This means that the nucleation of the dual additive systems is greatly dependent on the composition of NJ.

**Table 1. Values of Crystallization Temperature ($T_p$) and $\beta$-Crystal Form Content ($k_\beta$) versus Cooling Rate For iPP/IF-$WS_2$/NJ Nanocomposites**[a]

| IF-$WS_2$ content (wt.%) | NJ content (wt.%) | relative NJ content° | cooling rate (°C/min) | $T_p$ (°C) | $k_{\beta,\mathrm{WAXS}}$ |
|---|---|---|---|---|---|
| 0.0 | 0.0 | 0.0 | 01 | 118.1 | |
| | | | 02 | 115.2 | |
| | | | 05 | 110.6 | |
| | | | 10 | 106.9 | |
| | | | 20 | 102.8 | |
| 1.0 | 0.0 | 0.0 | 01 | 130.9 | |
| | | | 02 | 128.0 | |
| | | | 05 | 123.0 | |
| | | | 10 | 119.1 | |
| | | | 20 | 113.7 | |
| 1.0 | 0.05 | 0.048 | 01 | 131.1 | |
| | | | 02 | 128.8 | 0.67 |
| | | | 05 | 123.9 | 0.62 |
| | | | 10 | 120.5 | 0.58 |
| | | | 20 | 115.0 | 0.54 |
| 1.0 | 0.25 | 0.2 | 01 | 132.7 | |
| | | | 02 | 130.5 | 0.79 |
| | | | 05 | 126.8 | 0.73 |
| | | | 10 | 123.2 | 0.65 |
| | | | 20 | 118.9 | 0.59 |
| 1.0 | 0.5 | 0.33 | 01 | 133.2 | |
| | | | 02 | 130.9 | |
| | | | 05 | 129.8 | |
| | | | 10 | 123.2 | |
| | | | 20 | 118.7 | |
| 1.0 | 1.0 | 0.5 | 01 | 133.2 | |
| | | | 02 | 130.7 | 0.80 |
| | | | 05 | 126.8 | 0.72 |
| | | | 10 | 123.2 | 0.69 |
| | | | 20 | 118.5 | 0.63 |
| 0.0 | 0.1 | 1.0 | 01 | 134.8 | |
| | | | 02 | 133.0 | 0.86 |
| | | | 05 | 129.0 | 0.80 |
| | | | 10 | 125.9 | 0.74 |
| | | | 20 | 121.4 | 0.72 |

[a] NJ (wt.%)/[IF-$WS_2$ (wt.%) + NJ(wt.%)].


dx.doi.org/10.1021/jp2058194 |J. Phys. Chem. B 2011, 115, 10836–10843

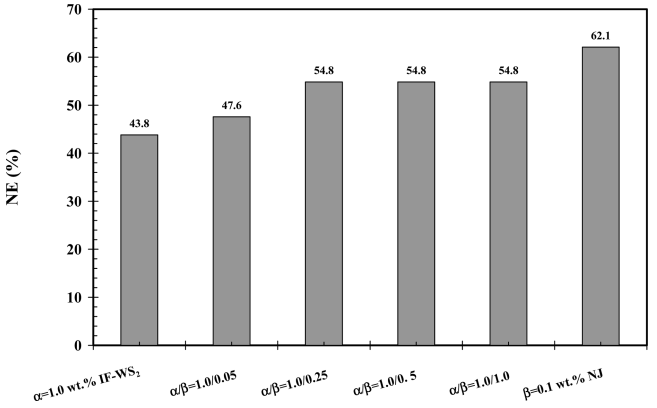


**Figure 3.** Nucleating efficiency (*NE*) of iPP nucleated with $\alpha$(IF-$WS_2$)/$\beta$(NJ) and individual $\alpha$ or $\beta$ NA.

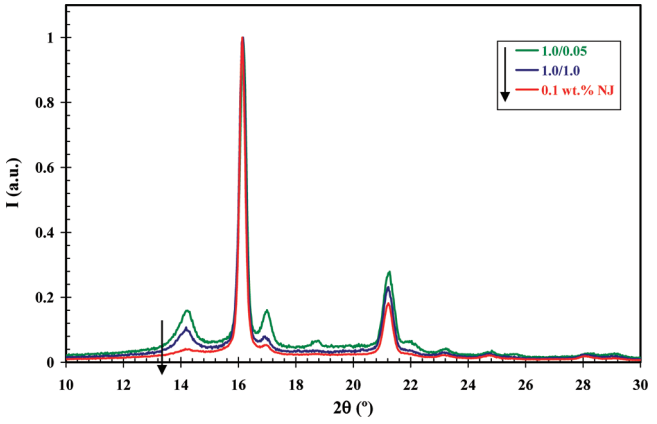


**Figure 4.** WAXS diffractograms of iPP nucleated with $\alpha$(IF-$WS_2$)/$\beta$(NJ) NA and individual $\beta$ NA obtained during cooling from the melt to room temperature at 20 °C/min.

**3.2. Nucleation Efficiency of the Individual and Dual $\alpha$(IF-$WS_2$)/$\beta$(NJ) Additive Systems.** To gain insight into the crystallization behavior of the iPP/IF-$WS_2$/NJ nanocomposites, the nucleation efficiency (NE) of the dual additive *NAs*, $\alpha$(IF-$WS_2$)/$\beta$(NJ), was estimated based on the methodology developed by Fillon et al.[39,40] according the following equation:

$$\mathrm{NE}(\%) = 100 \times \frac{T_{\mathrm{cNA}} - T_{\mathrm{c1}}}{T_{\mathrm{c2max}} - T_{\mathrm{c1}}} \qquad (5)$$

where $T_{\mathrm{cNA}}$, $T_{\mathrm{c1}}$, and $T_{\mathrm{c2max}}$ are peak crystallization temperatures of the nucleated, non-nucleated and self-nucleated polymer, respectively. It should be noted that the Fillon method assumes that with self-nucleation the highest crystallization temperature is achieved. Thus, the crystallization temperature of a non-nucleated polymer is considered as the lower boundary of the nucleation efficiency scale and that of the self-nucleated polymer as the upper boundary. The efficiency of heterogeneous nucleation, induced by adding the nucleating agent, should lie between that of homogeneous nucleation and self-nucleation. According to this scale, the NE of nucleated iPP by individual and dual $\alpha$(IF-$WS_2$)/$\beta$(NJ) additive systems was calculated considering a value of $T_{\mathrm{c2max}}$ = 140 °C,[4] and the results are shown in Figure 3 for a cooling rate of 10 °C/min. Clearly, for iPP nucleated with $\alpha$(IF-$WS_2$)/$\beta$(NJ), the NE is higher than that of iPP/IF-$WS_2$ but still lower than that of iPP/NJ. When the relative content of NJ is less than 20%, the NE value increases rapidly and then remains constant with further increase in the ratio. If the difference in NE for the two NAs is not pronounced, then competitive nucleation occurs, which can explain the nucleation process of $\alpha$(IF-$WS_2$)/$\beta$(NJ). In particular, the estimated NE for iPP nucleated by different NAs agrees well with the variation of $T_{\mathrm{p}}$ observed during the cooling process.

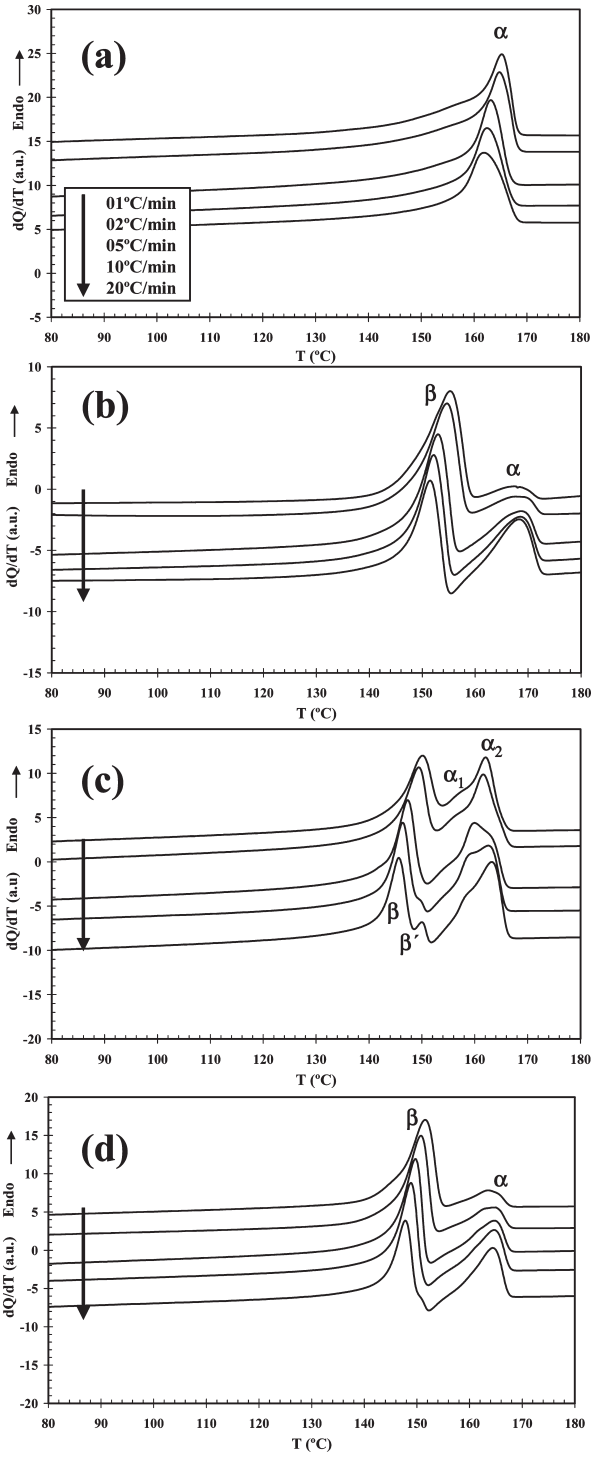


**Figure 5.** DSC thermograms of iPP nucleated with individual and dual $\alpha/\beta$ NAs obtained at heating at 5 °C/min after dynamic crystallization at the cooling rates indicated: (a) $\alpha$(1.0 wt.% IF-$WS_2$), (b) $\beta$(0.1 wt.% NJ), (c) $\alpha/\beta$(1.0/0.05 wt.%), and (d) $\alpha/\beta$(1.0/1.0 wt.%).


dx.doi.org/10.1021/jp2058194 |*J. Phys. Chem. B* 2011, 115, 10836–10843

Table 2. Values of Melting Temperature and Crystallinity versus Cooling Rate for iPP/IF-$WS_2$/NJ Nanocomposites

| IF-$WS_2$ content (wt.%) | NJ content (wt.%) | cooling rate (°C/min) | $T_{m,\beta}$ (°C) | $T_{m,\alpha}$ (°C) | $(1-\lambda)_\beta$ | $(1-\lambda)_\alpha$ | $k_{\beta,DSC}$ |
|---|---|---|---|---|---|---|---|
| 1.0 | 0.0 | 01 | | 165.2 | | 0.62 | |
| | | 02 | | 164.8 | | 0.63 | |
| | | 05 | | 163.2 | | 0.64 | |
| | | 10 | | 162.7 | | 0.66 | |
| | | 20 | | 161.9 | | 0.68 | |
| 1.0 | 0.05 | 01 | 150.1 | 157.2/163.6 | 0.42 | 0.17 | 0.71 |
| | | 02 | 149.4 | 157.1/162.0 | 0.35 | 0.23 | 0.69 |
| | | 05 | 147.4 | 161.9/163.0 | 0.32 | 0.29 | 0.63 |
| | | 10 | 146.4/149.7 | 160.0/162.6 | 0.30 | 0.29 | 0.60 |
| | | 20 | 145.6/150.1 | 160.1/163.2 | 0.33 | 0.29 | 0.55 |
| 1.0 | 0.25 | 01 | 151.1 | 163.1 | 0.55 | 0.10 | 0.83 |
| | | 02 | 150.3 | 162.8 | 0.51 | 0.12 | 0.80 |
| | | 05 | 149.2 | 164.0 | 0.46 | 0.17 | 0.71 |
| | | 10 | 148.3 | 164.0 | 0.40 | 0.20 | 0.65 |
| | | 20 | 147.4 | 163.9 | 0.34 | 0.24 | 0.58 |
| 1.0 | 0.5 | 01 | 151.2 | 162.9 | 0.50 | 0.14 | 0.78 |
| | | 02 | 150.4 | 162.7 | 0.47 | 0.16 | 0.73 |
| | | 05 | 149.1 | 161.9 | 0.39 | 0.19 | 0.66 |
| | | 10 | 148.3 | 163.7 | 0.35 | 0.22 | 0.61 |
| | | 20 | 147.3 | 163.8 | 0.32 | 0.25 | 0.55 |
| 1.0 | 1.0 | 01 | 151.6 | 163.6 | 0.51 | 0.08 | 0.85 |
| | | 02 | 150.8 | 165.0 | 0.46 | 0.11 | 0.81 |
| | | 05 | 149.7 | 164.7 | 0.47 | 0.16 | 0.74 |
| | | 10 | 148.9 | 164.7 | 0.41 | 0.19 | 0.67 |
| | | 20 | 147.8 | 164.4 | 0.38 | 0.23 | 0.61 |
| 0.0 | 0.1 | 01 | 155.3 | 167.5 | 0.49 | 0.05 | 0.90 |
| | | 02 | 154.7 | 167.8 | 0.48 | 0.08 | 0.86 |
| | | 05 | 153.0 | 168.6 | 0.43 | 0.13 | 0.78 |
| | | 10 | 152.2 | 168.5 | 0.38 | 0.17 | 0.69 |
| | | 20 | 151.5 | 168.4 | 0.31 | 0.20 | 0.59 |

**3.3. Influence of the Cooling Rate and $\alpha$(IF-$WS_2$)/$\beta$(NJ) Concentration on the Crystal Structure of iPP.** WAXS was employed to estimate the quantity of the $\beta$-phase of iPP. Figure 4 shows the normalized WAXS diffractograms of nucleated iPP with IF-$WS_2$(1.0 wt.%)/NJ(0.05 wt.%), IF-$WS_2$(1.0 wt.%)/NJ(1.0 wt.%), and NJ (0.1 wt.%) nonisothermally crystallized at a cooling rate of 20 °C/min. In this profile, (110) at $2\theta$ = 14.1°, (040) at 16.9°, (130) at 18.8° are the principal reflections of the $\alpha$-crystals of iPP, while (300) at about 16° is the principle reflection of the $\beta$-crystals used for normalization. These are considered as the marker peaks for the $\alpha$- and $\beta$-crystalline forms, respectively. Consistent with the results from DSC, only $\alpha$-crystals exist in neat iPP and iPP nucleated by IF-$WS_2$. Compared to that of pure iPP, an obvious difference can be seen in the diffractogram of iPP nucleated by NJ and the dual $\alpha/\beta$ system, where the intensities of the reflections of the $\alpha$-form clearly diminish with increasing NJ content. The result shows that both the individual $\beta$ NAs and the dual $\alpha/\beta$ NAs induce the $\beta$-form of iPP. The relative content of $\beta$-crystals ($k_{\beta,WAXS}$) was calculated according to eq 4 (Table 1), and it was seen that NJ induced a large amount of $\beta$-crystals while IF-$WS_2$ only induced $\alpha$-crystals. Clearly for the dual additive nucleated iPP the relative content of the $\beta$-phase is dependent not only on the cooling rate, but also on the relative content of $\alpha$ and $\beta$ NAs, as is further discussed in the following section.

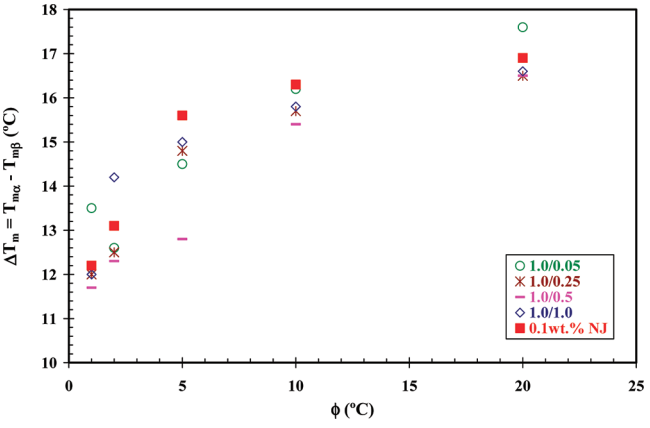


**Figure 6.** Variation of $\Delta T_m = T_{m\alpha} - T_{m\beta}$ with cooling rate ($\phi$) of iPP nucleated with dual $\alpha/\beta$ (1.0/0.05, 1.0/0.25, 1.0/0.5, and 1.0/1.0 wt.%) and individual $\beta$ NA (NJ = 0.1 wt.%).

**3.4. Influence of the Cooling Rate and $\alpha$(IF-$WS_2$)/$\beta$(NJ) Concentration on the Melting Behavior of iPP.** DSC can also be used to investigate the role of the thermal history on the polymorphic behavior of iPP nucleated with dual $\alpha$(IF-$WS_2$)/$\beta$(NJ) NAs and individual $\alpha$ or $\beta$ NAs. Figure 5 shows the DSC


dx.doi.org/10.1021/jp2058194 |J. Phys. Chem. B 2011, 115, 10836–10843

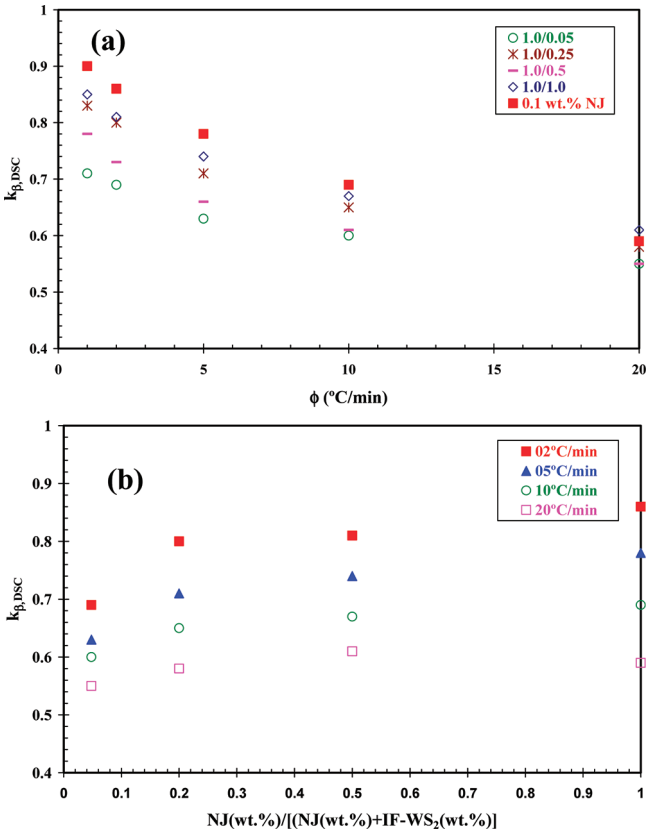


**Figure 7.** Variation of the relative content of $\beta$-crystals ($k_{\beta,DSC}$) with (a) the cooling rate and (b) the relative NJ content for iPP nucleated with $\alpha$(IF-WS$_2$)/$\beta$(NJ) NA and individual $\beta$ NA.

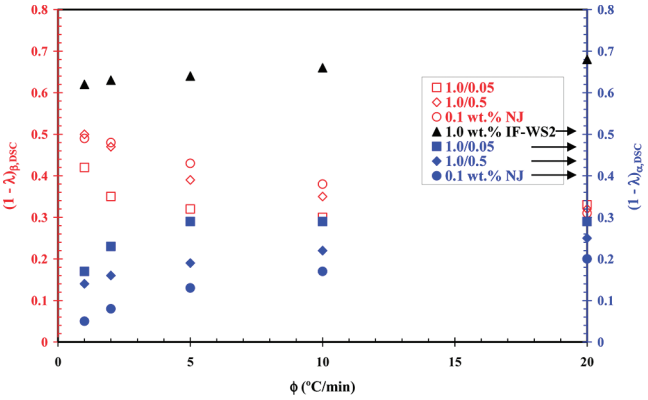


**Figure 8.** Variation of crystallinity of $\alpha$ and $\beta$ crystal forms with cooling rate for iPP systems indicated.

melting thermograms recorded at 5 °C/min subsequent to crystallization from the melt at various cooling rates, and the data are listed in Table 2. As an example, Figure 5a shows the effects of the crystallization cooling rate on the melting behavior of iPP/IF-WS$_2$ (1.0 wt.%). Only one melting peak is observed at around 160−165 °C, corresponding to the melting of the $\alpha$-phase, which means that only $\alpha$-crystals form during the dynamic crystallization process.[24] With decreasing cooling rate, the endotherm located at 160 °C gradually increases to higher temperature. This is because slower cooling rates favor the improvement of the size and perfection of the monoclinic $\alpha$-form crystals. However, for 0.1wt.% NJ nucleated iPP, two melting peaks are observed at approximately 151−155 °C and 167−169 °C, indicating the melting of $\beta$-phase and $\alpha$-phase,[6] respectively, Figure 5b. It is evident that the size of the melting peak for the $\beta$-crystals increased for slower cooling rates of dynamic crystallization, while the $\alpha$-crystal content consistently decreased, and the melting peak of the $\beta$-crystals shifted to higher temperature when cooling rate was reduced. This is attributed to the increase in size and perfection of the $\beta$-crystals when the crystallization occurs at a lower cooling rate. Furthermore, in the case of the melting curves obtained after cooling at 10 and 20 °C/min, it is possible to observe an exothermic transition at 155−156 °C immediately after the melting of the $\beta$-crystals. These results suggest that $\beta$-nucleated iPP samples are susceptible to a $\beta-\alpha$ recrystallization transition[41,42] before the melting of the $\alpha$ polymorph that originated from monoclinic crystals generated during secondary crystallization in the cooling process.[6,12,43−47] Finally, in the region of high temperature there is a broad endotherm representing the melting of the monoclinic $\alpha$-crystals formed during both the cooling process as well as those originating from the $\beta-\alpha$ transformation, previously commented.

In the case of iPP nucleated by $\alpha$(IF-WS$_2$)/$\beta$(NJ), the melting behavior subsequent to the melt-crystallization process is strongly dependent not only on the cooling rate, but also on the relative content of $\alpha$ and $\beta$ NAs. As a comparison, Figure 5c shows the melting thermograms of iPP nucleated with 1.0 wt % of IF-WS$_2$ and 0.05 wt % NJ. It can be clearly seen that the characteristic peaks of the $\beta$-phase located at 145−150 °C gradually increase with decreasing cooling rates, corresponding to the melting of progressively larger $\beta$-crystals. To the best of our knowledge, it is impossible to achieve 100% $\beta$-phase in the crystallization of iPP, and the $\beta$-phase is unstable. This fact leads to the formation of a poorly developed peak at 150 °C at cooling rates of 10 and 20 °C/min, related to the $\beta-\beta'$ transition. The observation of this transformation indicates the presence of a perfection or structural stabilization phenomenon of the trigonal $\beta$-crystals developed during the cooling from the melt that does not involve a transition between different crystalline forms. Thus, the existence of a $\beta-\beta'$ transformation is representative of a high structural instability in the trigonal $\beta$-phase.[41,42] Similarly, the melting behavior of the $\alpha$-phase is also influenced by the cooling rate. In particular, when the melting temperature is higher than 150 °C, a broad heterogeneous endotherm was observed, whose shoulder appears to be highly dependent on the cooling rate. This endotherm is associated with the melting of monoclinic crystals with different levels of perfection and crystal sizes. These crystals are susceptible to recrystallization and reorganization phenomena during heating, giving rise to the formation of larger/more perfect crystals, whose melting peak corresponds to the maximum endotherm located at high temperature.[48−50] In addition, underneath this endotherm the melting of the monoclinic $\alpha$-crystals generated from the $\beta-\alpha$ transformation during heating must also be considered. However, when the relative concentration of $\beta$ NAs increases, e.g., IF-WS$_2$/NJ = 1.0/1.0 wt %, the melting behavior observed was slightly different, Figure 5d. In this case, the $\beta-\beta'$ transition was not observable at high cooling rates, the melting and recrystallization phenomenon of the monoclinic crystals was less apparent, and the relation between the endothermic peak areas associated with the melting of $\alpha$ and $\beta$ crystals was larger due to the presence of a higher concentration of $\beta$ NA. Obviously, the difference between the melting temperature


dx.doi.org/10.1021/jp2058194 |J. Phys. Chem. B 2011, 115, 10836–10843

of trigonal and monoclinic phases progressively diminished when the cooling rate was reduced (Figure 6), a process leading to the reduction in the capacity for and level of recrystallization, reflected in a reduction of the endothermic peak area associated with the melting of the $\alpha$-crystals.

However, DSC can also be used to estimate the amount of $\beta$-crystals of iPP from the DSC melting thermograms, according to eq 3. Figure 7 shows the variation of the $k_{\beta,DSC}$ values versus cooling rate and relative $\beta$(NJ) content. Obviously, the relative content of the $\beta$-phase is dependent on the cooling conditions (Figure 7a): lower cooling rates favor the growth of the $\beta$-phase.[6,17−19] In addition, the $k_{\beta,DSC}$ values are also affected by the relative NJ content at all cooling rates. This effect is clearly observed to be a function of the composition (Figure 7.b). When the relative NJ content is less than 20%, the $k_{\beta,DSC}$ values increase and then remain constant with further increase of this parameter, in close agreement with the values of $k_{\beta,WAXS}$, from X-ray scattering.

To further verify the influence of the cooling rate on the evolution of the polymorphic behavior, crystallinity values of the $\alpha$-crystal form, $(1\text{-}\lambda)_\alpha$, and $\beta$-crystal form, $(1\text{-}\lambda)_\beta$, were calculated from the heating thermograms of nucleated iPP systems using eqs 1 and 2. Figure 8 shows the evolution of these for iPP/$\alpha$(IF-$WS_2$)/$\beta$(NJ) systems crystallized at various cooling rates. It is clear that as the cooling rate of the crystallization process increases, the degree of crystallinity of the $\beta$-phase diminishes and the degree of crystallinity of the $\alpha$-phase increases, i.e., transformation of $\beta$ to $\alpha$, especially for iPP nucleated with $\alpha$(IF-$WS_2$)/$\beta$(NJ) systems in comparison with individual $\alpha$ and $\beta$ NAs. This effect is less pronounced in the case of iPP nucleated with a low concentration of $\beta$(NJ) NA, which demonstrates the competition between both types of heterogeneous nucleation.

## 4. CONCLUSIONS

The dynamic crystallization and melting behavior of nucleated isotactic polypropylene (iPP) with $\alpha$(IF-$WS_2$)/$\beta$(NJ) have been comparatively studied in this work. The cooling rate and $\beta$(NJ) content were shown to be very efficient factors for the control of the dynamic crystallization behavior and the final crystalline structures in nucleated iPP. Our results showed that iPP crystallization via incorporation of a $\beta$-nucleating agent is energetically favored and remarkably increases the crystallization rate of iPP. The nucleating characteristics of $\alpha$(IF-$WS_2$)/$\beta$(NJ) can be illustrated by competitive nucleation. The presence of a highly $\beta$-nucleating agent played a leading role during iPP crystallization even at low weight ratios, inducing a progressive inhibition of the $\alpha$-nucleating effect of IF-$WS_2$ on the matrix. The content of $\beta$-crystals could be modulated by adjusting the IF-$WS_2$ and NJ composition ratio and controlling the cooling rate. In this case, for a specific $\alpha$-nucleating agent content (i.e., 1.0 wt. %), only a very low concentration of about 0.05 wt.% was required to obtain a significant fraction of the crystalline $\beta$-phase (54−67%). Further increase in the $\beta$-nucleant concentration, progressively increased the fraction of $\beta$-phase to practically reach limiting values at 0.1 wt % NJ (72−86%). The melting behavior of the nucleated iPP was also analyzed, and the influence of the cooling rate and NJ content on the transformation from a multimodal DSC melting peak to a bimodal one was established. It was shown that the magnitude and location of $\beta\beta'$ and $\alpha_1\alpha_2$ transitions were strongly controlled by the cooling rate and additive composition. In particular, the difference between the melting temperature of trigonal and monoclinic phases was found to diminish with slower cooling rate, a process leading to the reduction of the capacity and level of the $\beta-\alpha$ transformation. This effect was also corroborated by the results on the evolution of the crystallinities of the $\alpha$ and $\beta$ phases. As the cooling rate of the crystallization process increased, the degree of crystallinity of the $\beta$-phase diminished and the degree of crystallinity of the $\alpha$-phase increased, especially for iPP nucleated with the dual $\alpha$(IF-$WS_2$)/$\beta$(NJ) additive system, with this effect being less pronounced in the presence of a low concentration of the $\beta$-nucleant.

## AUTHOR INFORMATION

**Corresponding Author**
*E-mail: mnaffakh@ictp.csic.es.

## ACKNOWLEDGMENT

This work was supported by the Spanish Ministry of Science and Innovation, MICINN (Project: MAT2010-21070-C02-01), and by the European Commission for the X-ray synchrotron experiments performed at the Soft Condensed Matter A2 beamline at HASYLAB (DESY-Hamburg, Project: I-20100101 EC). Dr. M. Naffakh would like to express thanks to the Consejo Superior de Investigaciones Cientificas (CSIC) for an Intramural Research Fellowship (under Project No. 201160E003).

## REFERENCES

(1) Beck, H. N. *J. Appl. Polym. Sci.* **1967**, *11*, 673–685.
(2) Binsbergen, F. L.; De Lange, B. G. M. *Polymer* **1970**, *11*, 309–332.
(3) Wittmann, J. C.; Lotz, B. *J. Polym. Sci., Polym. Phys. Ed.* **1981**, *19*, 1837–1851.
(4) Marco, C.; Ellis, G.; Gómez, M. A.; Arribas, J. M. *J. Appl. Polym. Sci.* **2002**, *84*, 1669–1679.
(5) Marco, C.; Ellis, G.; Gómez, M. A.; Arribas, J. M. *J. Appl. Polym. Sci.* **2002**, *84*, 2440–2450.
(6) Marco, C.; Ellis, G.; Gómez, M. A.; Arribas, J. M. *J. Appl. Polym. Sci.* **2002**, *86*, 531–539.
(7) Blomenhofer, M.; Ganzleben, S.; Hanft, D.; Schmidt, H. W. *Macromolecules* **2005**, *38*, 3688–3695.
(8) Thierry, A.; Straupé, C.; Wittmann, J. C.; Lotz, B. *Macromol. Symp.* **2006**, *241*, 103–110.
(9) Libster, D.; Aserin, A.; Garti, N. *Polym. Adv. Technol.* **2007**, *18*, 685–695.
(10) Jacoby, P.; Bersted, B. H.; Kissel, W. J.; Smith, C. E. *J. Polym. Sci., Part B: Polym. Phys.* **1986**, *24*, 461–491.
(11) Tjong, S. C.; Shen, J. S.; Li, R. K. Y. *Polym. Eng. Sci.* **1996**, *36*, 100–105.
(12) Karger-Kocsis, J.; Varga, J. *J. Appl. Polym. Sci.* **1996**, *62*, 291–300.
(13) Tordjeman, Ph.; Robert, C.; Marin, G.; Gerard, P. *Eur. Phys. J. E* **2001**, *4*, 459–465.
(14) Marco, C.; Gómez, M. A.; Ellis, G.; Arribas, J. M. *Recent Res. Devel. Appl. Polym. Sci.* **2002**, *1*, 587–610.
(15) Sterzynski, T.; Oysaed, H. *Polym. Eng. Sci.* **2004**, *44*, 352–361.
(16) Zhang, Y. F.; Xin., Z. *J. Polym. Sci., Part B: Polym. Phys.* **2007**, *45*, 590–596.
(17) Zhang, Y. F. *J. Polym. Sci., Part B: Polym. Phys.* **2008**, *46*, 911–916.
(18) Bai, H.; Wang, Y.; Liu, L.; Zhang, J.; Han, L. *J. Polym. Sci., Part B: Polym. Phys.* **2008**, *46*, 1853–1867.
(19) Zhao, S.; Xin, Z. *J. Polym. Sci., Part B: Polym. Phys.* **2010**, *48*, 653–655.
(20) Manias, E.; Touny, A.; Wu, L.; Strawhecker, K.; Lu, B.; Chung, T. C. *Chem. Mater.* **2001**, *13*, 3516–3523.

(21) Chan, C. M.; Wu, J. S.; Li, J. X.; Cheung, Y. K. *Polymer* **2002**, *43*, 2981–2992.
(22) Manchado, M. A. L.; Valentini, L.; Biagiotti, J.; Kenny, J. M. *Carbon* **2005**, *43*, 1499–1505.
(23) Marco, C.; Naffakh, M.; Gómez, M. A.; Santoro, G.; Ellis, G. *Polym. Compos.* **2011**, *32*, 324–333.
(24) Naffakh, M.; Martín, Z.; Fanegas, N.; Marco, C.; Gómez, M. A.; Jiménez, I. *J. Polym. Sci., Part B: Polym. Phys.* **2007**, *45*, 2309–2321.
(25) Naffakh, M.; Martín, Z.; Marco, C.; Gómez, M. A.; Jiménez *Thermochim. Acta* **2008**, *472*, 11–16.
(26) Naffakh, M.; López, V.; Zamora, F.; Gómez, M. A. *Soft Mater.* **2010**, *8* (4), 407–425.
(27) Naffakh, M.; Remškar, M.; Marco, C.; Gómez-Fatou, M. A.; Jiménez., I. *J. Mater. Chem.* **2011**, *21*, 3574–3578.
(28) Chen, B.; Evans, J. R. G. *Soft Matter* **2009**, *5*, 3572–3584.
(29) Naffakh, M.; Marco, C.; Gómez, M. A. J; Jiménez, I. *J. Phys. Chem. B* **2009**, *113*, 7107–7115.
(30) Naffakh, M.; Diez-Pascual, A. M.; Marco, C.; Gómez, M. A.; Jiménez, I. *J. Phys. Chem. B* **2010**, *114*, 11444–11453.
(31) Naffakh, M.; Marco, C.; Gómez, M. A. J; Jiménez, I. *Mater. Chem. Phys.* **2011**, *128*, 265–273.
(32) Tang, J.; Wang, Y.; Liu, H.; Belfiore, L. A. *Polymer* **2004**, *45*, 2081–2091.
(33) Ghugare, S. V.; Govindaiah, P.; Avadhani, C. V. *Polym. Bull.* **2009**, *63*, 897–909.
(34) Chen, H.; Wang, M.; Lin, Y.; Chan, C. M.; Wu, J. *J. Appl. Polym. Sci.* **2007**, *106*, 3409–3416.
(35) Naffakh, M.; Díez-Pascual, A. M.; Gómez-Fatou, M. A. *J. Mater. Chem.* **2011**, *21*, 7425–7433.
(36) Li, X.; Cheung, W. L. *Polymer* **1998**, *39*, 6935–6940.
(37) Li, J. X.; Cheung, W. L.; Demin, J. *Polymer* **1999**, *40*, 1219–1222.
(38) Turner-Jones, A.; Aizlewood, J. M.; Beckett, D. R. *Makromol. Chem.* **1964**, *75*, 134–159.
(39) Fillon, B.; Lotz, B.; Thierry, A.; Wittmann, J. C. *J. Polym. Sci. Polym. Phys.* **1993**, *31*, 1395–1405.
(40) Fillon, B.; Thierry, A.; Lotz, B.; Wittmann, J. C. *J. Therm. Anal. Cal.* **1994**, *42*, 721–731.
(41) Varga, J. *J. Therm. Anal.* **1986**, *31*, 165–172.
(42) Varga, J.; Gabor, G.; Ille, A. *Angew. Makromol. Chem.* **1986**, *142*, 171–181.
(43) Lovinger, A. J.; Chua, J. O.; Gryte, C. C. *J. Polym. Sci. Polym. Phys.* **1977**, *15*, 641–656.
(44) Rybnikar, F. *J. Macromol. Sci. Phys.* **1991**, *B30*, 201–223.
(45) Karger-Kocsis, J.; Shang, P. P. *J. Therm. Anal.* **1998**, *51*, 237–244.
(46) Varga, J. *J. Mater. Sci.* **1992**, *27*, 2557–2579.
(47) Varga, J. *J. Therm. Anal.* **1989**, *35*, 1891–1912.
(48) Samuels, R. J. *J. Appl. Polym. Sci.* **1975**, *13*, 1417–1446.
(49) Yadav, Y. S.; Jain, D. C. *Polymer* **1986**, *27*, 721–727.
(50) Petraccone, V.; Guerra, G.; De Rosa, C.; Tuzi, A. *Macromolecules* **1985**, *18*, 813–814.